



Oncolytic adeno-immunotherapy modulates the immune system enabling CAR T-cells to cure pancreatic tumors

Amanda Rosewell Shaw ^{1,2,4}, Caroline E. Porter^{1,2,4}, Tiffany Yip^{1,2}, Way-Champ Mah^{1,2}, Mary K. McKenna^{2,3}, Matthew Dysthe^{2,3}, Youngrock Jung^{1,2}, Robin Parihar^{2,3}, Malcolm K. Brenner^{1,2,3} & Masataka Suzuki ^{1,2}✉

High expression levels of human epidermal growth factor receptor 2 (HER2) have been associated with poor prognosis in patients with pancreatic adenocarcinoma (PDAC). However, HER2-targeting immunotherapies have been unsuccessful to date. Here we increase the breadth, potency, and duration of anti-PDAC HER2-specific CAR T-cell (HER2.CART) activity with an oncolytic adeno-immunotherapy that produces cytokine, immune checkpoint blockade, and a safety switch (CA*dTrio*). Combination treatment with CA*dTrio* and HER2.CARTs cured tumors in two PDAC xenograft models and produced durable tumor responses in humanized mice. Modifications to the tumor immune microenvironment contributed to the antitumor activity of our combination immunotherapy, as intratumoral CA*dTrio* treatment induced chemotaxis to enable HER2.CART migration to the tumor site. Using an advanced PDAC model in humanized mice, we found that local CA*dTrio* treatment of primary tumor stimulated systemic host immune responses that repolarized distant tumor microenvironments, improving HER2.CART anti-tumor activity. Overall, our data demonstrate that CA*dTrio* and HER2.CARTs provide complementary activities to eradicate metastatic PDAC and may represent a promising co-operative therapy for PDAC patients.

¹Department of Medicine, Section of Hematology/Oncology, Baylor College of Medicine, Houston, TX, USA. ²Center for Cell and Gene Therapy, Baylor College of Medicine, Texas Children's Hospital, Houston Methodist Hospital, Houston, TX, USA. ³Department of Pediatrics, Section of Hematology/Oncology, Baylor College of Medicine, Houston, TX, USA. ⁴These authors contributed equally: Amanda, Rosewell Shaw, Caroline E, Porter.

✉email: suzuki@bcm.edu

Pancreatic cancer is the seventh leading cause of cancer death worldwide and without new effective treatments will soon surpass the death rate of more common cancers¹. Pancreatic ductal adenocarcinoma (PDAC) tumors tend to have low mutational burden² and are classified as immunologically “cold” tumors with little immune cell activation within the immunosuppressive tumor microenvironment (TME)³. Thus, even in the era of cancer immunotherapy, PDAC patients rarely benefit from immunotherapies like checkpoint blockade³.

Oncolytic viruses (OVs) selectively replicate in and kill tumor cells and can induce immune cell infiltration at tumor sites through virus-mediated inflammatory responses⁴. Based on this unique feature, OVs have been investigated in PDAC patients to overcome limited immune infiltration into tumors. Talimogene laherparepvec (T-VEC), an oncolytic herpesvirus FDA-approved for the treatment of melanoma, showed some anti-tumor activity in patients with advanced pancreatic cancer; however, the study was terminated early due to the rate of patient progression⁵. Likewise, pelareorep, an oncolytic reovirus, tested in a phase II trial demonstrated safety but did not improve progression-free survival⁶. On the other hand chimeric antigen receptor-modified T cells (CAR T cells) are gaining attention as potential therapeutic options for PDAC patients. Although Mesothelin-specific CAR T cells demonstrated safety, they had limited anti-tumor activity in PDAC patients⁷. These clinical results indicate that single immunotherapy agents are insufficient to control PDAC tumor growth, and recent clinical trials for PDAC have combined different types of agents (e.g., combination of radiotherapy, chemotherapy, vaccine plus checkpoint inhibitors (NCT02648282)) to overcome multiple barriers to immunotherapy.

High HER2 expression is associated with poorer prognosis in PDAC patients⁸. In a phase II clinical trial, patients with metastatic PDAC with grade 3 HER2 expression by immunohistochemistry were treated with the HER2 monoclonal antibody Trastuzumab (Herceptin) in combination with fluorouracil⁹. This HER2-targeting therapy was tolerated but did not improve progression-free or overall survival in these patients.

We previously demonstrated that our combination immunotherapy strategy, which couples oncolytic adenoviral immunotherapy (CAAd)¹⁰ with clinically tested HER2-specific CAR T-cells (HER2.CART)^{11,12}, mediates significant anti-tumor effects against multiple solid tumors¹³. Our combination of CAAd expressing IL-12 and PD-L1 blocking antibody with HER2.CART improved long-term survival in an aggressive metastatic model of head and neck squamous cell carcinoma^{14,15}. Here, we tested whether our combination immunotherapy with HER2.CART and CAAd expressing IL-12, PD-L1 blocking antibody, and safety switch HSVtk (CAAd $Trio$) could resolve HER2-positive PDAC tumors.

We found that one clinically feasible dose of CAAd $Trio$ was unable to control tumor growth in PDAC xenograft mouse models. However, even local CAAd $Trio$ treatment stimulated systemic host immune responses to repolarize distant PDAC tumor microenvironments, additively improving HER2.CART anti-tumor activity to eradicate advanced PDAC tumors in humanized mice.

Results

HER2.CARTs and CAAd $Trio$ kill human PDAC lines in vitro.

Although monoclonal antibody therapy targeting HER2 previously failed for PDAC patients⁹, HER2.CARTs have higher avidity (multivalent versus bivalent) and ability to directly kill tumor cells through cytolytic proteins as opposed to antibody-dependent cellular cytotoxicity through infiltrating immune cells. We thus hypothesized that our clinically tested HER2.CARTs¹¹

could efficiently target HER2-positive PDAC tumors. We first confirmed that our HER2.CARTs effectively kill PDAC lines with varying levels of HER2 expression (Fig. 1a). Since PDAC patients have been safely treated with oncolytic viruses^{16,17}, we also confirmed that our oncolytic adeno-immunotherapy, comprised of an oncolytic adenovirus (OAd) and a helper-dependent adenoviral vector (HDAd) encoding human interleukin 12p70 (hIL12p70), programmed death ligand 1 (PDL1) blocking mini-antibody, and herpes simplex virus thymidine kinase (HSVtk) safety switch expression cassettes (CAAd $Trio$), lysed PDAC lines (Fig. 1b). We next assessed whether CAAd $Trio$ -infected PDAC lines amplified the transgenes encoded in HDAd (Fig. 1c, Supplementary Fig. 1). We found that CAAd $Trio$ induced oncolysis of PDAC lines at levels similar to OAd alone (Fig. 1b), and transgenes encoded in HDAd were significantly amplified in CAAd $Trio$ -infected PDAC cells compared to those infected with only HDAd (Fig. 1c). To test whether these transgenes improved HER2.CART killing, we co-cultured PDAC cells infected with HDAd $Trio$ (no lytic effect) with HER2.CART (Supplementary Fig. 2). We confirmed that HDAd-derived transgenes enhanced HER2.CART killing of PDAC cells in vitro, similar to other tumor types, even in the absence of adenoviral mediated oncolysis^{13,14}.

HER2.CARTs are the primary mediator of PDAC tumor control in xenograft models.

To evaluate the complementary benefits of CAAd $Trio$ and HER2.CARTs in vivo, mice with subcutaneous CFPAC-1 tumors received 1×10^7 viral particles (vp) of CAAd $Trio$ before being infused with 1×10^6 HER2.CARTs 3 days later (Fig. 2a). Although CAAd $Trio$ failed to control tumor growth, mice treated with either HER2.CART alone or combination of HER2.CART and CAAd $Trio$ both had consistent, complete, and sustained eradication of CFPAC-1 tumors (complete response: CR). In these CFPAC-1 mice we observed no difference in HER2.CART infiltration or expansion at the tumor site or circulating IFN γ levels in the blood of mice treated with either HER2.CART alone or combination therapy (Fig. 2b, c). Likewise, there was no difference in animal survival between HER2.CART alone and combination treatment (Fig. 2d). Although we detected CAAd $Trio$ -derived IL-12p70 in the blood (Fig. 2c), we found local CAAd treatment had no additive anti-tumor effect in CFPAC-1 xenograft mice.

To address whether the observed anti-tumor effects were unique to CFPAC-1, we evaluated the reproducibility of our results in a subcutaneous model of CAPAN-1 (Fig. 3a). CAAd $Trio$ alone showed little antitumor activity and we observed no statistical difference in survival between control and CAAd $Trio$ -treated mice (Fig. 3d). Similar to a previous study, we still detected Ad vectors in tumors (Supplementary Fig. 3a)¹⁰. Thus, CAAd $Trio$ is likely unable to control tumor growth in these xenograft models due to necrosis and disruption of tumor vasculature by oncolysis, which may prevent the continuous spread of viruses within the tumor mass¹⁰.

HER2.CART alone significantly controlled tumors compared to the control group. However, tumors recurred in two HER2.CART-treated mice due to antigen (HER2) loss (Supplementary Fig. 3b). We found, however, that combination treatment with CAAd $Trio$ and HER2.CART completely and consistently eradicated CAPAN-1 tumors without tumor relapse (CR). We also found that mice pre-treated with CAAd $Trio$ showed significantly higher HER2.CART infiltration/expansion ($p < 0.005$) at the tumor site within 7 days post infusion and increased circulating IFN γ ($p = 0.004$) in the blood compared to mice treated with HER2.CART alone at 7 days post infusion (Fig. 3b, c). These results indicate that oncolysis combined with PD-L1 blockade and IL-12 enhances the potency of adoptively transferred HER2.

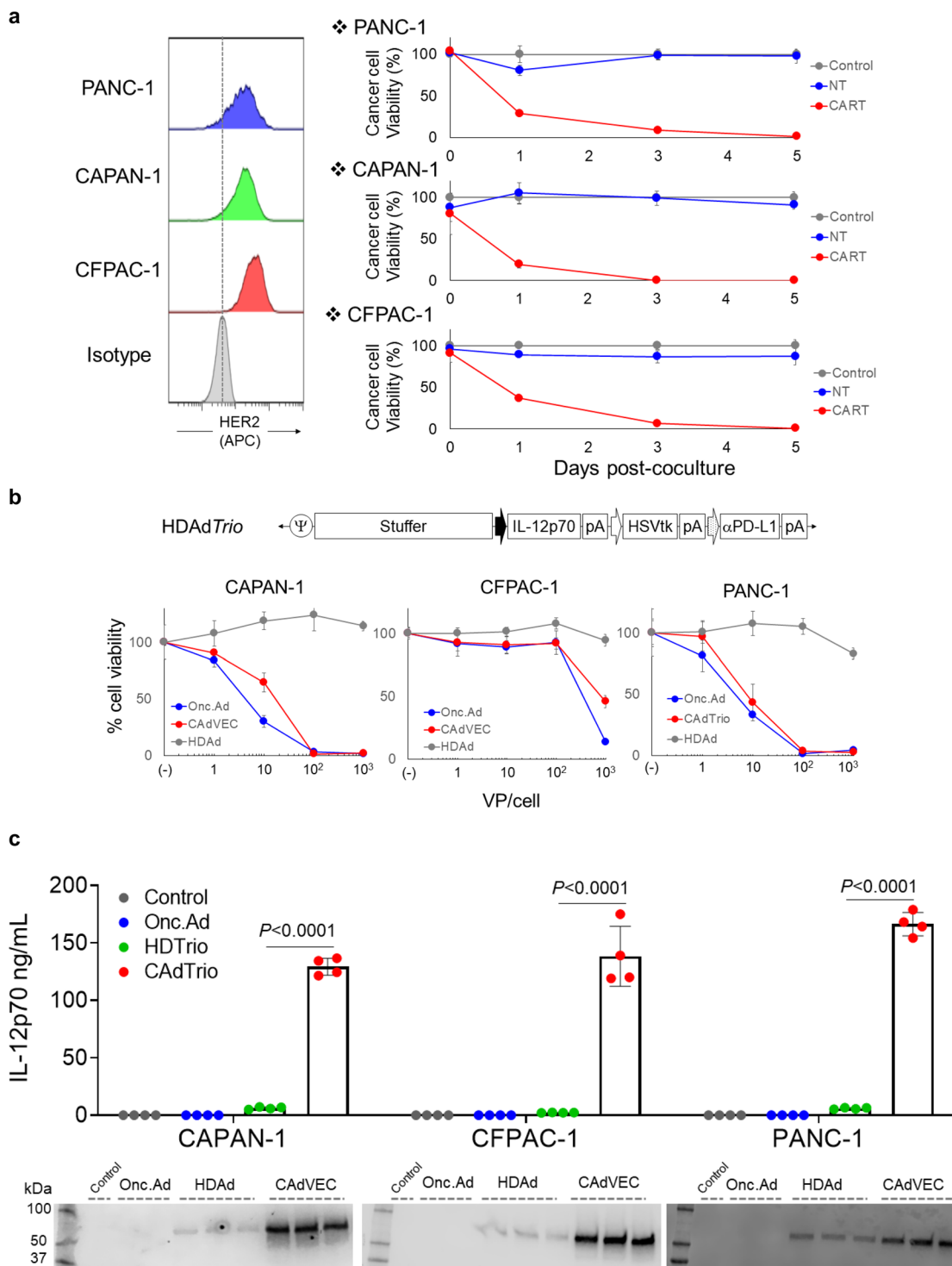


Fig. 1 HER2.CART and CADTrio kill human PDAC lines in vitro. **a** HER2 expression was analyzed by flow cytometry on PANC-1, CAPAN-1, and CFPAC-1. Tumor cells expressing *fluc* were cultured with NTs or HER2.CARTs (E:T = 1:10). Cells were harvested 0, 1, and 5 days post coculture, and viable cancer cells were analyzed by luciferase assay ($n = 4$ biologically independent samples, each time point). Data are presented as means \pm SD. **b** Schematic structure of HDAd encoding human IL-12p70, HSVtk safety switch and PDL1 blocking antibody expression cassettes (HDAdTrio). PANC-1, CAPAN-1, and CFPAC-1 were infected with increasing doses of HDAdTrio, OAd, or CAAdTrio (OAd: HDAd=1:1) ($n = 6$ biologically independent samples). We analyzed viable cells at 96 h by MTS assay. Data are presented as means \pm SD. **c** PANC-1, CAPAN-1, and CFPAC-1 were infected with total 10 vp/cell of HDAdTrio, OAd, or CAAdTrio (OAd:HDAd=1:1) ($n = 4$ biologically independent samples). We sampled media 48 h post infection and quantified levels of IL-12p70 and PD-L1 mini-antibody by IL-12p70 ELISA assay and Western blotting for PD-L1 mini-antibody, respectively. Data are presented as means \pm SD, $p < 0.0001$ determined by two-tailed t test ($t = 32.93$, $dF = 6$). Statistical significance set at $p < 0.05$, $ns > 0.05$.

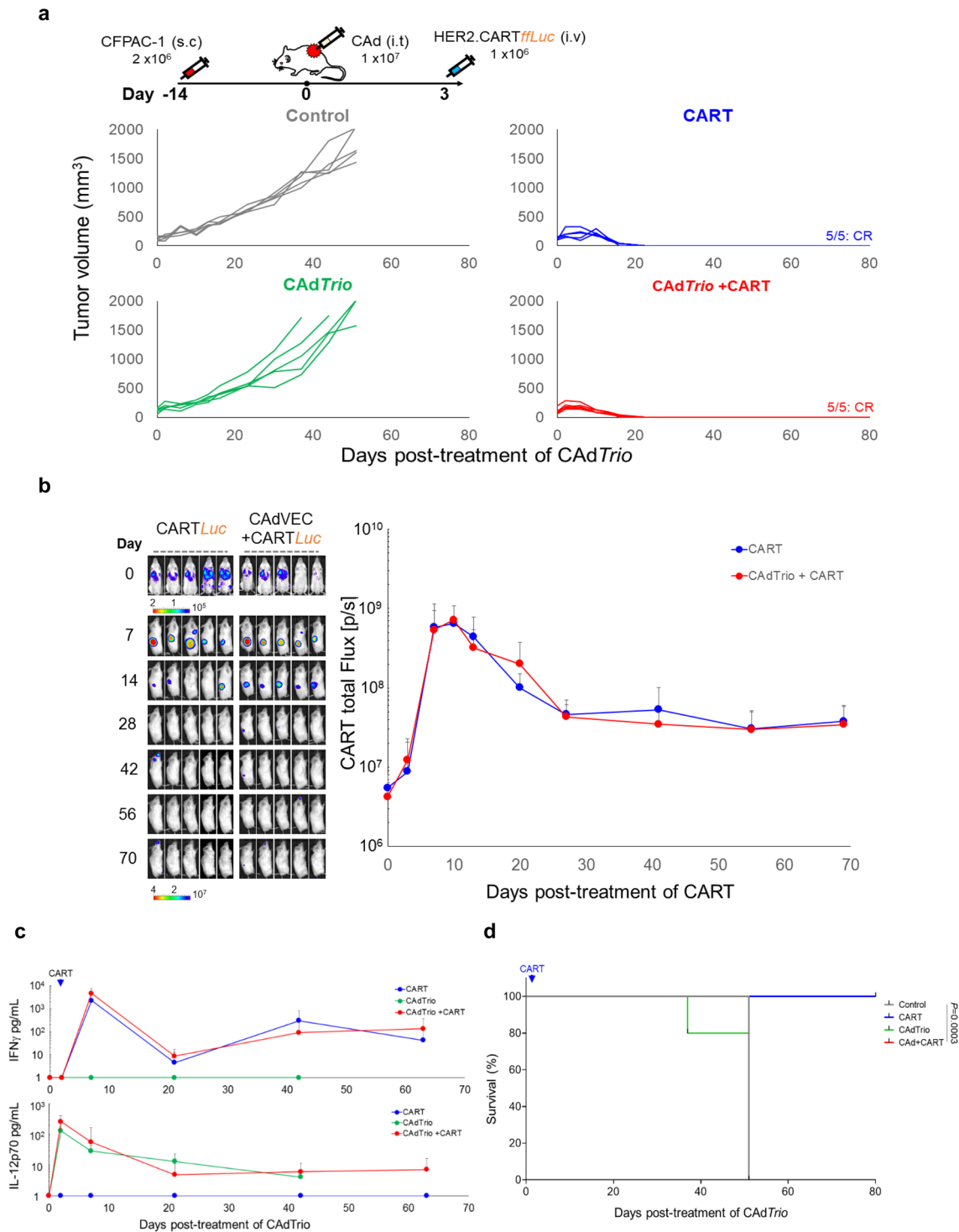


Fig. 2 HER2.CARTs primarily control CFPAC-1 tumor growth in xenograft mouse model. **a** CFPAC-1 cells were transplanted into the right flank of NSG mice ($n = 5$ animals). A total of 1×10^7 vp of CAdTrio (OAd:HD = 1:1) were injected i.t. A total of 1×10^6 HER2.CARTs expressing *ffLuc* were administered i.v. 3 days post injection of CAdTrio. Tumor volumes were monitored at different time points. **b** Bioluminescence of HER2.CARTs was monitored at the indicated time points. Data are presented as means \pm SD. **c** We collected serum samples from mice at 0, 3, 7, 21, 42, and 63 days post injection of CAdTrio, and measured IFN γ and IL-12p70 levels by ELISA. Data are presented as means \pm SD. **d** Kaplan-Meier survival curve after CAdTrio administration in mice ($n = 5$ animals) $p = 0.0003$. P -values were determined using the log-rank Mantel-Cox test ($df=3$). Statistical significance set at $p < 0.05$, ns > 0.05 . Abbreviations: s.c. subcutaneous, i.t. intratumoral, i.v. intravenous.

CARTs to control tumor growth in subcutaneous CAPAN-1 tumors. In this model, however, HER2.CART remained the major contributor to CAPAN-1 tumor control, as there was no significant difference in survival between HER2.CART alone and combination treatment (Fig. 3d). These results indicate that

HER2.CARTs effectively recognize and control PDAC tumor growth in vivo, and the additive effect of CAdTrio depends on the PDAC line. We did not observe autonomous HER2.CART expansion-related toxicity (e.g., weight loss) in these xenograft models (Supplementary Fig. 4).

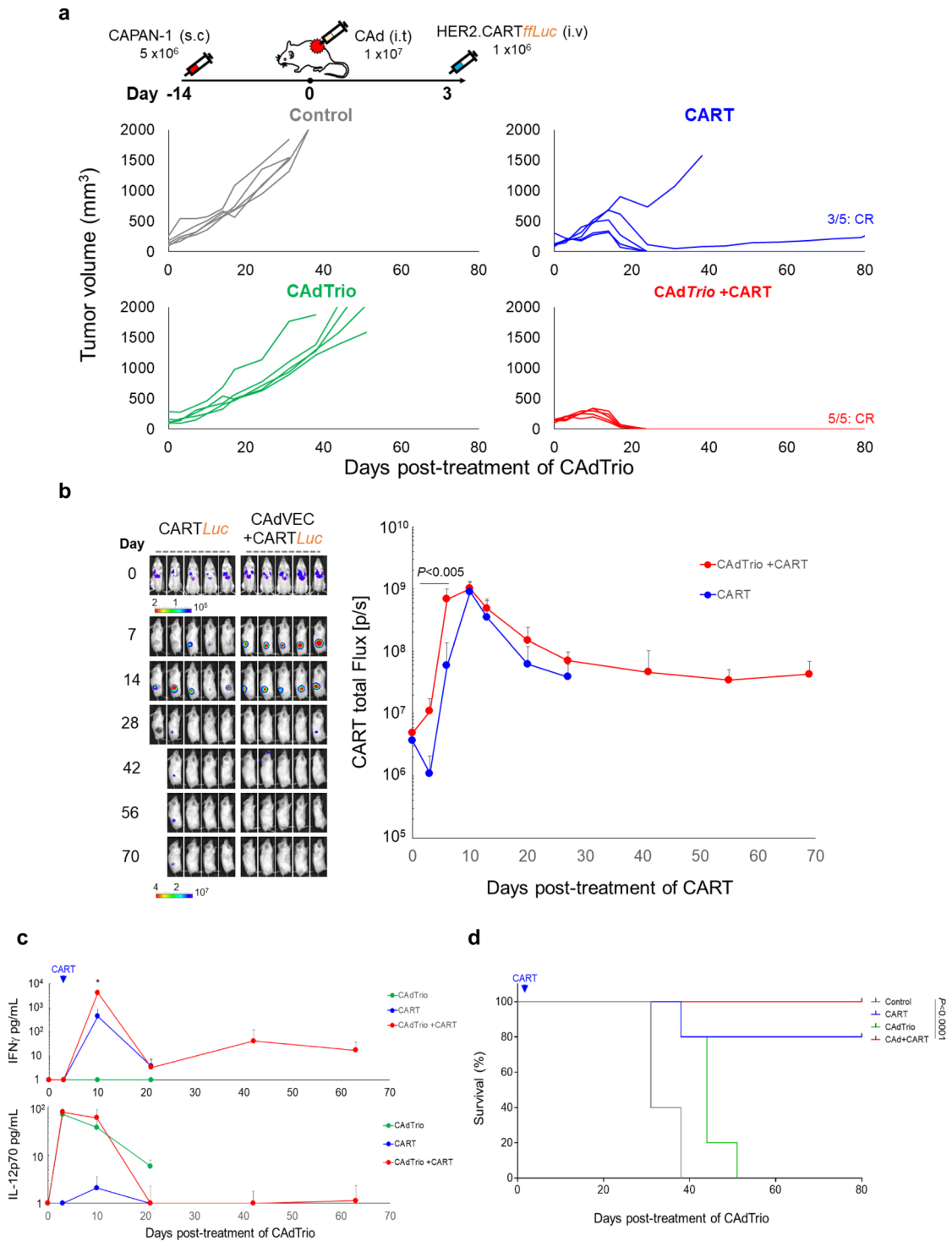


Fig. 3 HER2.CARTs primarily control CAPAN-1 tumor growth but require CadTrio to cure PDAC in xenograft mouse model. **a** CAPAN-1 cells were transplanted into the right flank of NSG mice ($n = 5$ animals). A total of 1×10^7 vp of CadTrio (OAd:HD = 1:1) were injected into the tumor. A total of 1×10^6 HER2.CARTs expressing *ffLuc* were systemically administered 3 days post injection of CadTrio. We monitored tumor volumes at different time points. **b** We monitored HER2.CART bioluminescence at different time points. Data are presented as means \pm SD, $p < 0.005$. P -values were determined by two-tailed t test ($t = 4.32$, $dF = 8$). **c** We collected serum samples from mice at 0, 3, 10, 24, 45, and 66 days post injection of CadTrio, and measured levels of IFN γ and IL-12p70 by ELISA. Data are presented as means \pm SD, $p = 0.004$. P -values were determined by two-tailed t test ($t = 5.769$, $dF = 8$). **d** Kaplan-Meier survival curve after CadTrio administration in mice ($n = 5$ animals), $p < 0.0001$. P -values were determined using the log-rank Mantel-Cox test ($dF = 3$). Statistical significance set at $p < 0.05$, $ns > 0.05$. Abbreviations: s.c. subcutaneous, i.t. intratumoral, i.v. intravenous.

Combination treatment is required to effectively control PDAC in humanized mice. The tumor microenvironment (TME) contributes to immunotherapy resistance in solid tumors, including PDAC¹⁸. To address whether our combination immunotherapy is required to overcome the protective TME, we evaluated its antitumor activity in immunocompetent animal models. Since human Ad-based Oads have limited infectivity (our Ads: serotype 3 knob) and replication in rodent cell lines^{19,20}, and our HER2.CAR construct was optimized for human T cells²¹, we reconstituted transgenic NSG mice ubiquitously expressing human SCF, IL-3, and GM-CSF (NSGSGM3) with human innate and adaptive immune cells using HLA-A2 cord blood unit (CBU)-derived CD34⁺ cells (Supplementary Fig. 5a)²². We then transplanted PDAC tumors into these humanized mice using CFPAC-1, which is HLA-A2 (Supplementary Fig. 5b). We found minimal systemic inflammation due to CFPAC-1 tumor formation with tumor-infiltrating human immune cells (Supplementary Fig. 5b, c), suggesting that these humanized mice tolerated CFPAC-1. To avoid allo-reaction to adoptively transferred HER2.CARTs, we generated HER2.CART from the same CBU-derived T cells (Supplementary Fig. 6a). These CBU-derived HER2.CARTs had phenotypes and CFPAC-1 killing similar to HER2.CART generated from healthy donor-derived PBMCs (Supplementary Fig. 6a).

After CFPAC-1 tumor formation, we treated mice with the same conditions as in the xenograft models: 1×10^7 vp *CAdTrio* and 1×10^6 autologous HER2.CARTs infused three days later (Fig. 4a). Although *CAdTrio* had no effect on CFPAC-1 tumors in our xenograft model (Fig. 2), in the humanized model *CAdTrio* alone led to significant ($p = 0.0002$) tumor control and prolonged survival ($p = 0.0107$) compared to the untreated control group (Supplementary Figs. 7 and 8). These results suggest that the host immune system, stimulated by *CAdTrio*, contributes to tumor control that cannot be seen in immunodeficient xenograft models where tumor control is primarily dependent on oncolysis. In contrast to the CFPAC-1 xenograft model (Fig. 2), HER2.CART alone delayed tumor control but did not cure all treated animals (Fig. 4a). In this humanized CFPAC-1 model, combination therapy had additive anti-tumor effects, with most treated mice achieving CR. There was no significant induction of pro-inflammatory cytokines (IL-6, TNF α , IL-1 β) or Th1-related cytokines (IFN γ , IL-2, IL-7) in the serum of humanized mice treated with single agents or combination treatment at early time points (Fig. 4b, Supplementary Fig. 9), indicating that these doses are well tolerated.

Due to lack of appropriate inflammatory and chemokine signals, CARTs show limited trafficking and infiltration to tumor sites in patients with solid tumors^{23,24}. We found that combination treatment significantly increased early HER2.CART infiltration to the tumor site ($p = 0.003$) compared to HER2.CART alone in humanized mice (Fig. 4c). Oncolytic virotherapy stimulates the host immune system through pattern recognition receptors and induces pro-inflammatory cytokine and chemokine expression^{25,26}. To address whether enhanced infiltration of HER2.CART was dependent on chemotaxis induced by *CAdTrio*, we harvested tumors 3 days post injection of *CAdTrio* (time at which CART would have been infused) and quantified pro-inflammatory RNA expression at the tumor site (Fig. 4d). Although *CAdTrio* did not induce pro-inflammatory genes in CFPAC-1 tumors in xenograft mice (lacking immune cells), in humanized mice, *CAdTrio* induced expression of type I IFN, IFN β ($p = 0.0093$), and type I IFN-dependent genes, including OAS1 ($p = 0.0004$), Mx1 ($p = 0.0005$), CCL5 (RANTES), and CXCL10 (IP10, $p = 0.0045$)^{27–30}. Since there was no significant difference in infiltrating immune subsets between untreated control and *CAdTrio*-treated humanized mice (Fig. 4e), these

results suggest that tumor-infiltrating immune cells recognize *CAdTrio* infection^{29,31} and stimulate the local immune system through type I IFN²⁹. This response also leads to expression of type II IFN, IFN γ , and IFN γ downstream genes (PD-L1, ICAM-1) at the tumor site (Fig. 4d)¹³. We confirmed that CBU-derived HER2.CARTs highly express chemokine receptors, CCR5 (for CCL5) and CXCR3 (for CXCL10) (Supplementary Fig. 6b). These results indicate that local *CAdTrio* treatment induces pro-inflammatory signals from the TME (but not CFPAC-1 cells themselves) and increases infiltration of adoptively transferred HER2.CART at the pre-treated tumor site, similar to a previous report³².

There was no autonomous expansion of adoptively transferred HER2.CART or induction of pro-inflammatory/Th1 cytokines in serum of humanized mice treated with combination immunotherapy, suggesting that *CAdTrio* locally enhances HER2.CART anti-tumor effects, leading to superior anti-tumor effects (Figs. 4a, 4 of 6 mice: CR) without systemic toxicity.

Combination treatment controls both *CAdTrio*-treated and untreated PDAC tumors in humanized mice.

Results from our humanized mouse model (Fig. 4) indicate that *CAdTrio* stimulates the host immune system and modulates the TME to recruit adoptively transferred HER2.CART to the tumor site. We thus hypothesized that *CAdTrio*-activation of the host immune system also modulates the TME at a distant tumor site (abscopal effect), leading distant tumor beds to respond to adoptively transferred HER2.CART. Since metastasis correlates with poor prognosis in PDAC patients³³, we gave our humanized mice a large (primary: right) and a small (metastatic: left) tumor to mimic metastatic disease, and treated only the right tumor with *CAdTrio* (Fig. 5a). Although both tumor sites in mice treated with HER2.CART alone showed HER2.CART infiltration 3 days post infusion (Fig. 5b), CART had limited expansion compared to the single tumor model, resulting in no significant tumor control compared to control mice (Supplementary Fig. 10). These results suggest that a threshold of CART infiltration is required to control CFPAC-1 tumor growth in humanized mice.

Local *CAdTrio* treatment controlled growth of the right (treated) tumor similar to our single tumor model but did not significantly control the left (untreated) tumor (Fig. 5a). However, even in this advanced tumor model, combination treatment completely eliminated right (*CAdTrio*-treated) tumors and significantly controlled distant tumor growth compared to other groups ($P < 0.01$) (Fig. 5a, Supplementary Fig. 10). Based on the *CAdTrio*-dependent chemotaxis observed in our single tumor model, we investigated HER2.CART infiltration at *CAdTrio*-treated tumor site (Fig. 5b). Combination treatment increased HER2.CART infiltration more at the right tumor than at the left at 3 days post infusion, but HER2.CART expanded at both sites equally after 14 days. Thus, improved HER2.CART infiltration and expansion leads to sustained anti-tumor effects even in *CAdTrio*-untreated tumors.

To address which *CAdTrio* components (oncolysis, IL-12 and PD-L1 blocking antibody) contribute to sustained anti-tumor effects with HER2.CART in humanized mice, we administered Cad0 (no transgene), *CAdPDL1* (PD-L1 blocking antibody), or *CAdIL12* (IL-12p70) (Supplementary Fig. 15) to the right tumor of humanized mice bearing two subcutaneous CFPAC-1 tumors, as in the previous experiment. Although each CAD component (oncolysis, PD-L1 blocking antibody or IL-12) provided some level of tumor control in both CAD-treated and untreated tumors when combined with HER2.CART, none eliminated the CAD-treated tumor. These results suggest that all components are required to control primary (large) tumor growth

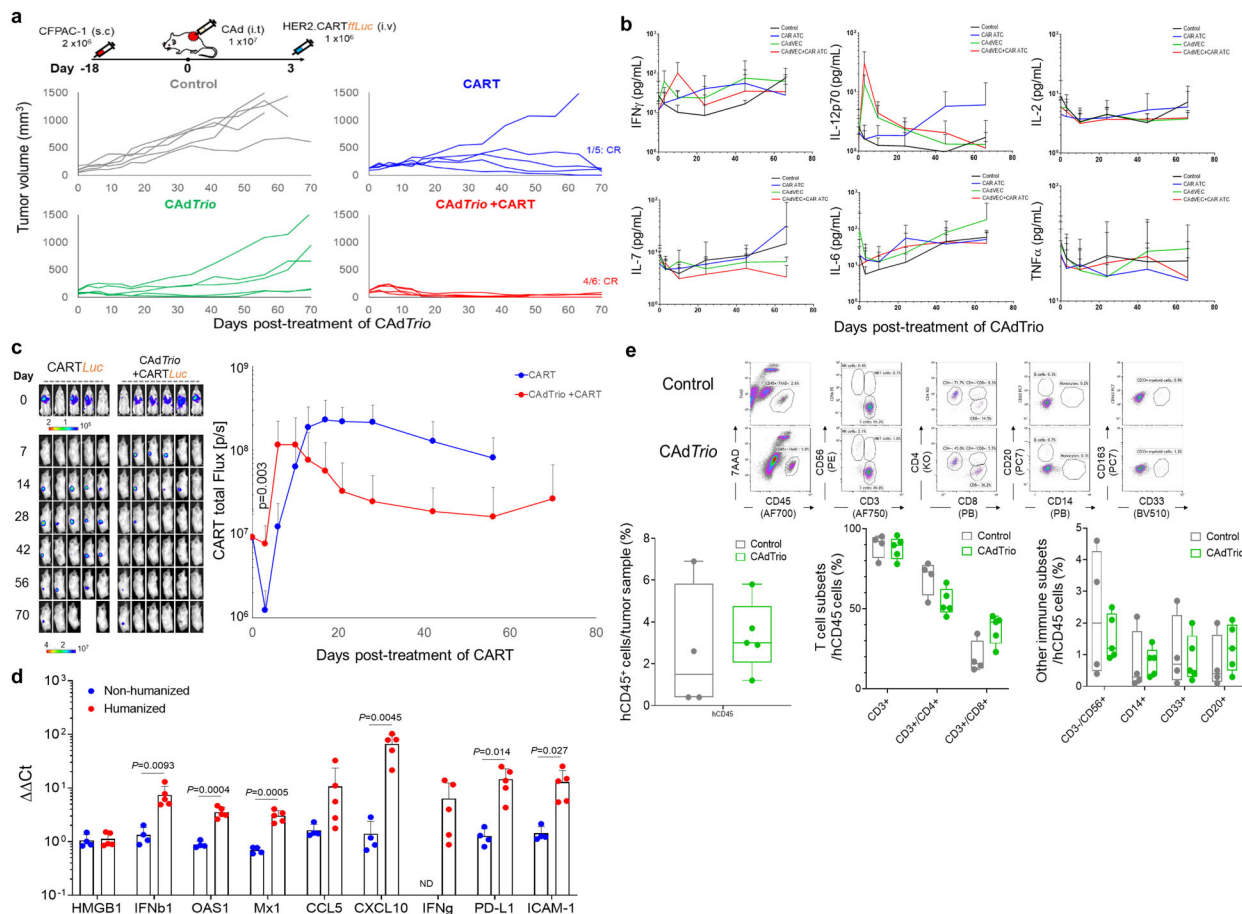


Fig. 4 Combination immunotherapy controls CFPAC-1 tumor growth in humanized mouse model. **a** CFPAC-1 cells were transplanted into the right flank of humanized mice (control, CART alone, *CadTrio* alone: $n = 5$ animals, *CadTrio*+CART: $n = 6$ animals). A total of 1×10^7 vp of *CadTrio* (OAd:HD = 1:1) were injected into the tumor. A total of 1×10^6 HER2.CARTs expressing *fluc* were systemically administered 3 days post injection of *CadTrio*. Tumor volumes were monitored at different time points. **b** We collected serum samples from mice at 0, 3, 10, 24, 45, and 66 days post injection of *CadTrio*, and measured human Th1 and Th2 cytokine levels by Multiplex. Data are presented as means \pm SD. **c** Bioluminescence of HER2.CARTs was monitored at different time points. Data are presented as means \pm SD, $p = 0.003$. P -values were determined using two-tailed t test (t ratio = 4.213, $df = 8$). **d** CFPAC-1 tumors were harvested from non-humanized and humanized mice (non-humanized mice: $n = 4$ animals, humanized mice: $n = 5$ animals) at 3 days post injection of *CadTrio*, and total RNA was extracted from whole tumors. Pro-inflammatory genes were quantified and normalized with human β -Actin. Data are presented as means \pm SD. P -values were determined using two-tailed t test; $p = 0.0093$ (t ratio = 3.553, $df = 7$), $p = 0.0004$ (t ratio = 6.352, $df = 7$), $p = 0.0005$ (t ratio = 6.084, $df = 7$), $p = 0.0045$ (t ratio = 4.101, $df = 7$), $p = 0.014$ (t ratio = 3.226, $df = 7$), $p = 0.027$ (t ratio = 2.782, $df = 7$). Statistical significance set at $p < 0.05$, ns > 0.05 . **e** CFPAC-1 tumors were harvested from humanized mice (non-humanized mice: $n = 4$ animals, humanized mice: $n = 5$ animals) at 3 days post injection of *CadTrio*, and tumor infiltrating human immune cells were analyzed with flow cytometry. Box plot elements: central line, median; box limit, upper and lower quartiles; whisker, 1.5x inter-quartile range; points, outliers. Abbreviations: s.c. subcutaneous, i.t. intratumoral, i.v. intravenous, ND not detectable.

(Supplementary Fig. 15a). In this experiment, we additionally evaluated HER2.CART distribution and found initial HER2.CART infiltration and expansion in *CadIL12*-treated mice was lower than that in mice treated with *CadTrio* ($p < 0.01$) (Supplementary Fig. 15b), similar to our previous experiments with xenograft mouse models^{14,15}. These data suggest that, while IL-12 may be the primary component of *CadTrio* to induce HER2.CART infiltration and expansion, all *CadTrio* components are required to maximize adoptively transferred HER2.CART infiltration and expansion at the primary tumor site and subsequent control of distant (*Cad*-untreated) tumors in humanized mice.

To compare how the treatments impact immune phenotypes, we euthanized all mice when control groups reached euthanasia criteria and phenotyped infiltrating immune cells in residual tumors (Fig. 5c, Supplementary Figs. 11, 12, and 13a). We found that mice treated with combination immunotherapy showed

higher endogenous human immune cell ($CD45^+$, EGFP⁺) infiltration than other groups in their left (*CadTrio*-untreated) tumors ($p = 0.0009$). However, there was no significant difference in the proportional composition of immune subsets (T cells, NK cells, monocytes, B cells) following combination immunotherapy compared to other groups. To address the correlation between immune cell infiltration and tumor immune gene signatures, we profiled the human immune gene expression signature of residual tumors (Fig. 5d, Supplementary Fig. 13b, Supplementary Data 1 and 2). Although there were no adenoviral vectors in the *CadTrio*-untreated (left) tumors (Supplementary Fig. 14a), we found that type I IFN- and Th1-related genes were upregulated in the left tumors of mice treated with *CadTrio* alone (but to a lesser degree than in right tumors), suggesting that local *CadTrio* treatment stimulates systemic host immune responses against CFPAC-1 tumors. Since HER2.CARTs infiltrated both tumor sites in the absence of *CadTrio* pre-treatment as well (Fig. 5b),

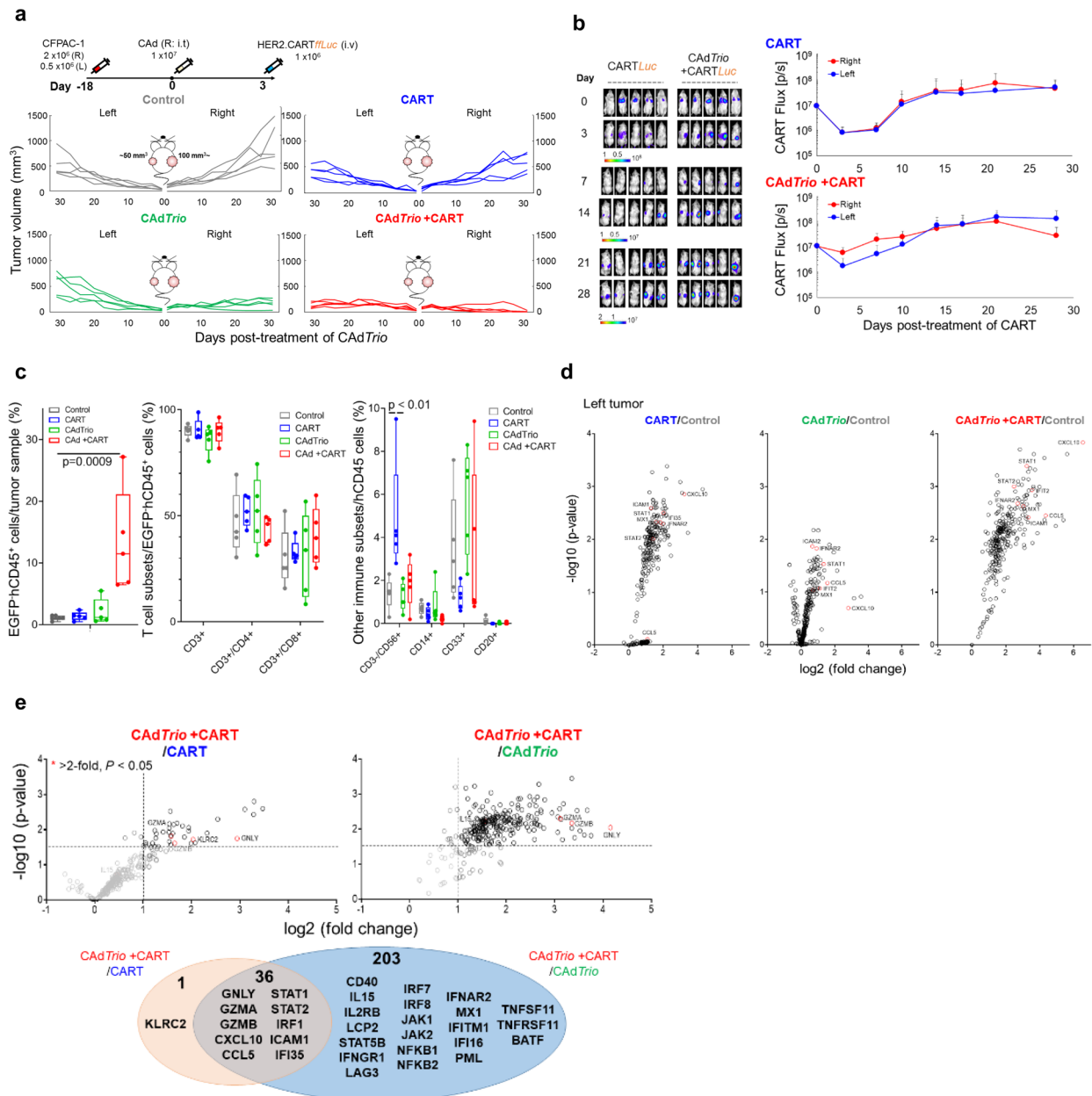
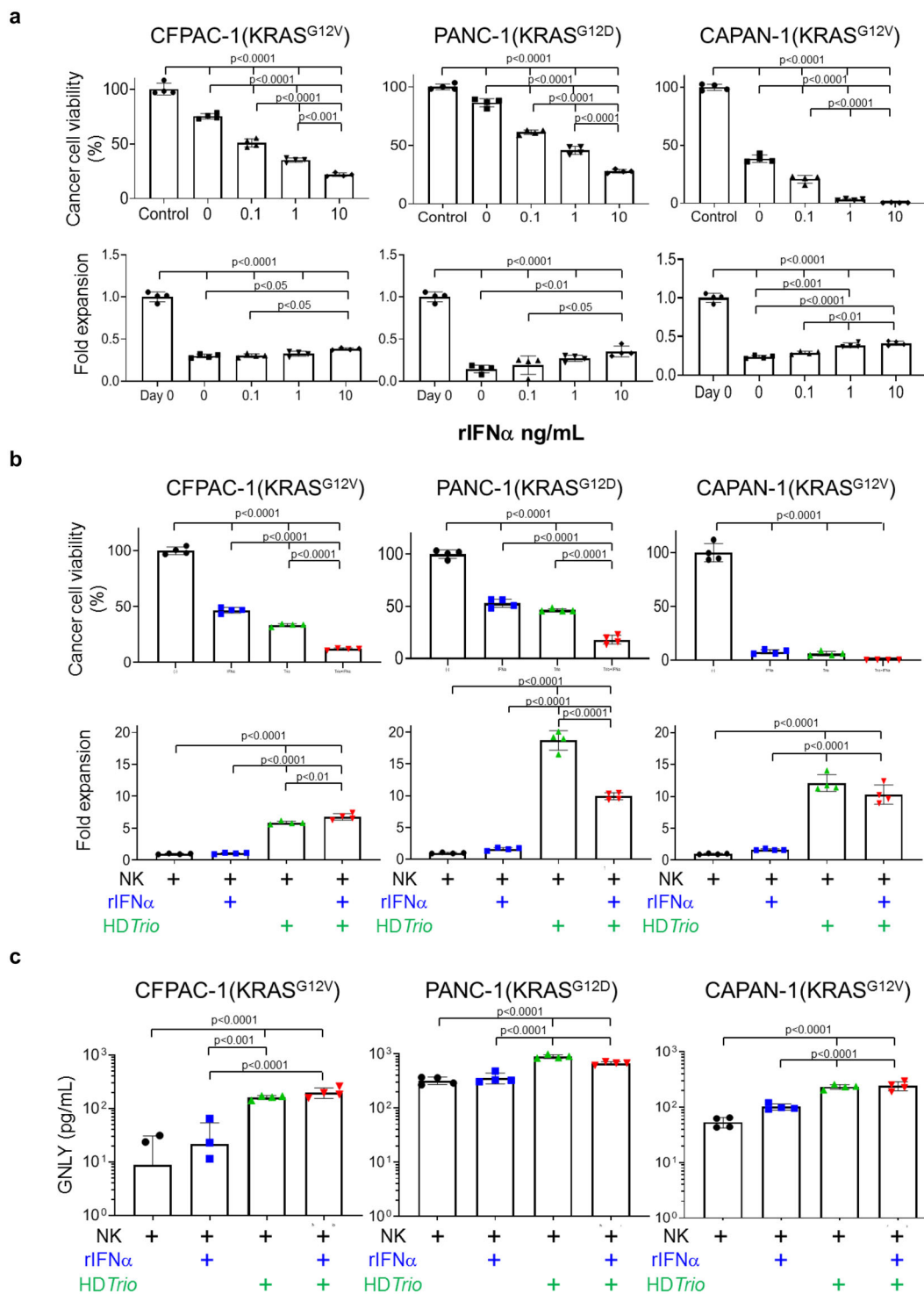


Fig. 5 Combination immunotherapy controls tumor growth in humanized mice with multiple PDAC tumors. **a** CFPAC-1 cells were transplanted into the right and left flanks of humanized mice ($n = 5$ animals). A total of 1×10^7 vp of CadTrio (Oad:HD = 1:1) were injected into the right tumor. A total of 1×10^6 HER2.CARTs expressing *fluc* were systemically administered 3 days post injection of CadTrio. Tumor volumes were monitored at different time points. **b** Bioluminescence of HER2.CARTs was monitored at different time points. Data are presented as means \pm SD. **c** CFPAC-1 tumors were harvested from humanized mice at 31 days post injection of CadTrio, and tumor infiltrating human immune cells were analyzed by flow cytometry. Box plot elements: central line, median; box limit, upper and lower quartiles; whisker, 1.5x inter-quartile range; points, outliers. *P*-values were determined using ordinary one-way ANOVA with Tukey multiple comparisons, $p = 0.0009$ ($F(3,16) = 9.252$), $p < 0.01$ ($F(3,16) = 6.426$). Statistical significance set at $p < 0.05$, ns > 0.05 . Total RNA was extracted from whole tumor at 31 days post injection of CadTrio. Gene expression was profiled with Nanostring, differential gene expression compared to control tumors (**d**) and compared to single agents (**e**) are shown. Abbreviations: s.c. subcutaneous, i.t. intratumoral, i.v. intravenous.

left tumors also expressed pro-inflammatory genes in the HER2. CART only condition (Fig. 5d). However, residual left tumors in mice treated with combination immunotherapy expressed higher levels of pro-inflammatory genes compared to mice treated with single therapies (Fig. 5d, Supplementary Data 1), and gene expression correlated with increased immune cell infiltration.

To address whether CadTrio or HER2.CART primarily induced pro-inflammatory gene expression in residual tumors, we compared gene expression between combination and single

treatment profiles (Fig. 5e, Supplementary Data 3). We found that 239 genes were significantly upregulated in combination treatment compared to CadTrio alone. Of these 239 genes, 36 genes upregulated in the combination group were associated with both CadTrio and HER2.CART treatments. These 36 genes included a range of cytotoxic molecules such as Granulysin, Granzyme A and B. Only one gene (KLRC2 (NKG2C)) was uniquely upregulated in a CadTrio-dependent manner (significantly upregulated in combination compared to HER2.CART alone).



NK cells enhance anti-PDAC activity in the presence of type I IFN and *CadTrio*. Although *KLRC2* is primarily expressed in NK cells and effector CD8⁺ T cells^{34,35} we found *KLRC2* upregulation 3 days after injection of *CadTrio* and before injection of HER2.CARTs (Supplementary Fig. 16). Since lack of type I IFN signaling in NK cells impairs their cytotoxic function in different tumor models³⁶ and *CadTrio*-treated tumors upregulated type I IFN, we hypothesized that type I IFN induced by immunomodulatory molecules derived from *CadTrio* enhance the anti-PDAC activity of NK cells. We tested NK cell anti-PDAC activity using PDAC lines in the presence of recombinant type I IFN (rIFN α) in vitro (Fig. 6a). We found that rIFN α increased the

anti-PDAC activity of NK cells in a dose-dependent manner, yet having little effect on proliferation. Although rIFN α alone induced some cancer cell death (Supplementary Fig. 17), our results overall indicate that type I IFN enhances NK cell anti-PDAC activity. As IL-12 and PD-L1 blockade are also associated with improved NK cell anti-tumor activity^{37,38}, we next examined whether *CadTrio*-derived IL-12 and PD-L1 blocker additively increased NK cell anti-PDAC activity (Fig. 6b). We found that these molecules enhanced NK cell anti-PDAC activity irrespective of the presence of IFN α , and independently induced NK cell proliferation. We next measured the cytotoxic molecule granulysin (GNLY) in media of these co-culture experiments, since

Fig. 6 NK cells enhance anti-PDAC activity in the presence of type I IFN and immunomodulatory molecules from CADTrio. **a** PANC-1, CAPAN-1, and CFPAC-1 expressing *ffLuc* were cultured with NK cells with increasing doses of rIFN α . We also cultured NK cells expressing *ffLuc* with these cancer cells (E:T = 1:10) with increasing doses of rIFN α . Cells were harvested 0 and 72 h post coculture, and viable cells were analyzed by luciferase assay ($n = 4$ biologically independent samples, each timepoint). Data are presented as means \pm SD. P -values were determined by ordinary one-way ANOVA with Tukey multiple comparisons. CFPAC ($F(4,15) = 351.8$) NK ($F(4,15) = 346.8$), Panc1 ($F(4,15) = 468.7$) NK ($F(4,15) = 106.3$), CAPAN1 ($F(4,15) = 1121$) NK ($F(4,15) = 318.4$). **b** PANC-1, CAPAN-1, and CFPAC-1 expressing *ffLuc* (or not expressing) were infected with 100 vp/cell of HDAdTrio. Cells expressing *ffLuc* were cultured with NK cells (E:T = 1:10). We also cultured NK cells expressing *ffLuc* with these cancer cells (E:T = 1:10) at 24 h post infection of HDAdTrio in the presence or absence of 1 ng/mL rIFN α . Cells were harvested 72 h post coculture, and viable cells were analyzed by luciferase assay ($n = 4$ biologically independent samples). Data are presented as means \pm SD. P -values were determined by ordinary one-way ANOVA with Tukey multiple comparisons. CFPAC ($F(3,12) = 1114$) NK ($F(3,12) = 458.3$), Panc1 ($F(3,12) = 356.6$) NK ($F(3,12) = 410.2$), CAPAN1 ($F(3,12) = 459.6$) NK ($F(3,12) = 131.4$). **c** We sampled media 72 h post coculture, and measured granulysin using ELISA assay ($n = 4$ biologically independent samples). Data are presented as means \pm SD. P -values were determined by ordinary one-way ANOVA with Tukey multiple comparisons, $p < 0.001$ ($F(3,12) = 41.07$), $p < 0.0001$ ($F(3,12) = 74.40$), $p < 0.0001$ ($F(3,12) = 49.49$). Statistical significance set at $p < 0.05$, ns > 0.05 .

GNLY can be induced by CADTrio in humanized mice (Fig. 5e, Supplementary Fig. 16) and GNLY-expressing NK cells may be a prognostic marker of solid tumor responses to recombinant IFN α (rIFN α) therapy³⁴. Although rIFN α slightly but not significantly increased GNLY levels in media compared to NK cells cocultured with PDAC alone, we found significantly increased levels ($p < 0.0001$) of GNLY in media in the presence of CADTrio components (IL-12 and PD-L1 blocker), irrespective of rIFN α (Fig. 6c). These results indicate that GNLY expression from NK cells is primarily dependent on CADTrio. Hence, type I IFN induced by CADTrio treatment, combined with CADTrio-expressed IL-12 and PD-L1 blocker, augments the activity and expansion of endogenous NK cells.

Overall, these studies indicate that CADTrio treatment leads to additive host immune stimulation including NK cells against PDAC to aid adoptively transferred HER2.CART in the control of PDAC tumor growth.

Discussion

Overall, we demonstrate that combining CADTrio and HER2.CARTs is a curative immunotherapy in several PDAC models, including humanized mouse models.

One major limitation of CAR T cells for solid tumor treatment is the identification of cell membrane targets with high-level, homogenous expression on solid tumors and limited expression on normal cells³⁹. CART can recognize antigens with relatively low expression due to higher overall avidity than antibodies, and our center has safely treated more than 36 patients with HER2-positive solid tumors with our HER2.CARTs^{11,12}. A recent study showed that patient-derived xenograft (PDX) PDACs expressed targetable levels of HER2 by HER2.CARTs, and they also found that PDAC cancer-stem cells (CSCs) express similar levels of HER2 as the non-CSC population⁴⁰. In this study, we found that our HER2.CARTs can recognize and kill PDAC lines expressing varying levels of HER2 in vitro and in vivo. However, we also found that tumors recurred in CAPAN-1 xenograft mice treated with HER2.CART alone due to antigen (HER2) loss, similar to what has been seen in CAPAN-1 xenograft mice treated with PSCA.CART⁴¹. These results suggest that CAPAN-1 attenuates the anti-tumor activity of single antigen-targeting CARTs with antigen loss independent of the target. Our combination treatment strategy quickly eradicates tumors overcoming the hurdle of antigen loss caused by protracted or incomplete tumor elimination by CAR T cells alone.

While CAR T-cell therapies for solid tumors have been effective in preclinical xenograft models, like our PDAC xenograft mice, several barriers to successful treatment exist in patients³⁹. For instance, limited trafficking of cell therapies to tumor sites may hamper effective treatment of solid tumors^{24,42}. We found

that delayed infiltration and expansion of HER2.CART at the tumor site attenuated anti-tumor activity in humanized mice. However, similar to another study using STING agonist³⁰, pre-treating tumors with CADTrio induced pro-inflammatory signals and chemotaxis, thereby improving CART infiltration within the tumor. Although we observed no significant difference in subsets of tumor-infiltrating lymphocytes between untreated control and CADTrio-treated tumors in humanized mice, CADTrio induced expression of type I IFN-related genes not detected in xenograft models. This finding suggests that IFN-related genes are activated in host immune cells, not tumor cells, and indicates that tumor-infiltrating immune cells recognize CADTrio components through pattern recognition receptors (e.g., TLR9^{29,31}) or are stimulated by CADTrio transgenes to induce pro-inflammatory responses. Metzger et al. demonstrated that type I IFN stimulation through TLR agonist repolarizes the PDAC TME, specifically myeloid-derived suppressor cells, in an immunocompetent KPC model⁴³. Although we did not see phenotypic differences with standard immune phenotype markers in this study, CADTrio treatment and the resulting induction of type I IFN may repolarize tumor-infiltrated immune cells to an immune activated state.

Metastatic disease is another barrier to successful immunotherapy for PDAC patients. Local oncolytic viro-immunotherapy is intended to augment systemic host anti-tumor effects by inducing potent abscopal immune responses^{44–46}. Given the inhibitory TME of human solid tumors, oncolytic virotherapy should be most effective against both injected and metastatic tumor sites when oncolysis is combined with relatively sustained immunostimulatory transgene expression⁴. Here, we used our CAD system to amplify the therapeutic transgenes encoded in HDAd with lytic effects provided through the OAd replication machinery¹⁰. Although the CADTrio dosage used in this study showed limited anti-tumor effects in xenograft models, we found that this dose, with immunostimulatory molecules derived from HDAd, activated the host immune system in humanized mouse models resulting in significant tumor control. To address whether local CADTrio treatment can systemically activate the host immune system and improve CART anti-tumor activity at a distant (untreated) site, we tested our combination immunotherapy in an advanced PDAC tumor model. Although HER2.CART primarily migrated to CADTrio-treated tumor sites, they also expanded at distant tumors in mice treated with combination immunotherapy to significantly control tumor growth compared to single agent treatments. Treating humanized mice with CAD expressing single components revealed IL-12 as the component of CADTrio most responsible for HER2.CART infiltration and expansion at the primary tumor site. However, none of the components alone eliminated the CAD-treated tumor or controlled distant tumor growth, as we observed in humanized mice treated with CADTrio.

Our studies suggest that all components are required to control both primary and distant tumor growth. In future studies, we will use our humanized mouse models and samples from our ongoing Phase I clinical trial (NCT03740256) to further characterize which *CAdTrio* component(s) by which mechanism(s) modify the PDAC TME and influence HER2.CART anti-tumor activity.

In addition to stimulating adoptively transferred HER2.CART, in humanized mice *CAdTrio* induced active (Th1) gene signatures at distant (untreated) tumor sites (abscopal effect), similar to what has been seen in melanoma patients treated with T-VEC⁴⁷. Therefore, *CAdTrio* treatment might make both tumor beds immunologically “hot” and thus susceptible to adoptively transferred HER2.CARTs. Combination treatment was required for significant control of distant tumors with relatively higher endogenous immune infiltration and type I IFN/Th1 related gene expression than other groups. However, single-cell RNA sequencing will be necessary to address which immune cells express these genes.

Based on immune gene signatures in residual tumors, we found that *KLRC2* (*NKG2C*) was uniquely upregulated in a *CAdTrio*-dependent manner. *KLRC2* is generally expressed on human NK cells and binds HLA-E molecules, indicators of adequate MHC class I expression by self cells⁴⁸. Clinically, *NKG2C*⁺ NK cells are indicators of good prognosis in CMV- and HIV-infected patients and have been implicated in innate memory³⁴. In cancer, increased infiltration of NK cells is associated with better prognosis in patients with solid tumors including PDAC^{49,50}. However, attenuated type I IFN signaling by pancreatic cancer harboring *KRAS* mutation and expressing *MYC* oncogene limits NK cell activity at PDAC tumor sites⁵¹. Our *in vitro* data indicates that exogenous type I IFN can restore NK cell anti-PDAC activity independent of *KRAS* mutation and that *CAdTrio* components directly enhanced NK cell anti-PDAC activity and proliferation. These data suggest that *CAdTrio* exerts both indirect (via type I IFN induction by host immune cells) and direct (via *IL12p70* and *PDL1* blocker components) effects on host NK cells that contribute to anti-tumor immunity in our humanized models.

In summary, we demonstrate that local provision of multiple immunomodulatory molecules as a *CAd* package augments the anti-tumor effects of adoptively transferred HER2.CARTs and endogenous immune cells (e.g., NK cells), allowing them to control both *CAdTrio*-treated and -untreated PDAC tumors. Oncolytic viro-immunotherapy also induces antigen-spread, leading to the development of tumor-associated antigen-specific cytotoxic T lymphocytes in patients⁴, an effect that cannot be fully replicated in our humanized mouse models due to limited thymic education/maturation⁵². Ultimately, clinical trials will reveal whether combination immunotherapy with *CAdTrio* and HER2.CART is sufficient for the desired systemic antitumor effects, including antigen spread. Analyses to address these questions are a major component of our Phase I clinical trial (NCT03740256) that has recruited its first patients following approval by the US Food and Drug Administration.

Methods

Adenoviral vectors (HDAdS and OAdS). The *IL-12p70*, HSV thymidine kinase (*HSVtk*), and PD-L1 blocking mini-antibody (anti-PD-L1 scFv sequence obtained from Tessa Therapeutics Pte.) expression cassettes (*IL-12p70* driven by EF1 promoter, *HSVtk* driven by hamster *GRP78* promoter, and PD-L1 mini-antibody driven by human *GRP94* promoter (InvivoGen)) were cloned into *pHDA21E4* (*HDAdTrio* vector). After confirming the sequence and expression of *IL12p70* (ELISA (BD Bioscience)), PD-L1 blocking mini-antibody (Western blotting with anti-HA IgG (Thermo Fisher Scientific)) and *HSVtk* (culturing cancer cells in the presence or absence of ganciclovir (GCV)), *HDAdTrio* were rescued with chimeric helper virus 5/3 (knob replacing Ad serotype 3 from Ad serotype 5) using 116 cells^{53,54}. We measured infectious units (IUs) of *HDAdTrio* using A549 cells⁵³. The IU of *HDAdTrio* used in this study was $\text{vp:IU} = 100:11$. *HDAd* without transgene

(*HDAd0*), *HDAd* expressing PD-L1 blocking antibody (*HDAdPDL1*), and *HDAd* expressing *IL-12p70* (*HDAdIL12*) were cloned into *pHDA28E4* vector and rescued in 116 cells^{10,13,14}. We substituted and cloned chimeric *OAd5/3Ad2E1AΔ24* (knob replacing Ad serotype 3 from Ad serotype 5) with *Ad5E1AΔ24* to *Ad2E1AΔ24* (deleting *pRb* binding site). We rescued *OAd5/3Ad2E1AΔ24* using 293 cells and propagated using A549 cells¹⁰. All unique materials are available from the authors upon request.

Cell lines. We obtained human pancreatic lines CAPAN-1, CFPAC-1, and PANC-1 from ATCC (Manassas, VA) in 2018. We authenticated cell lines with Short Tandem Repeat (STR) profiling by ATCC. Cells were cultured under the conditions recommended.

To generate cell lines expressing the fusion protein *EGFP-ffLuc*, we infected cells with retrovirus encoding *EGFP-ffLuc*^{13,14}. *EGFP*-positive cells were sorted using an SH800 Cell Sorter (Sony) after 3 passages post infection of retrovirus.

Primary cells. Human PBMCs were isolated using Ficoll-Paque Plus according to the manufacturer's instructions (Axis-Shield) from healthy donor whole blood (approved by the Baylor College of Medicine IRB Committee). The vector encoding the HER2-directed CAR incorporating the CD28 costimulatory endodomain (2nd generation *HER2.28ζ.CAR*)²¹, the fusion protein *EGFP-ffLuc*, and the methodology for the production of retrovirus and CARTs have been described previously¹¹. Briefly, PBMCs were activated with OKT3 (1 mg/ml) (Ortho Biotech) and CD28 antibodies (1 mg/ml) (Becton Dickinson) and fed every 2 days, beginning the day after stimulation, with media supplemented with 10 ng/mL of recombinant human interleukin-7 and 5 ng/mL of recombinant human interleukin-15 (rIL-7 and rIL-15, R&D). On day 2 post-OKT3/CD28 T blast generation, activated T cells ($0.125 \times 10^6/\text{mL}$) were added to CAR retroviral-coated plates and centrifuged at $400 \times g$ for 5 min. CAR-transduced T cells (*HER2.CARTs*) were expanded with media supplemented with 10 ng/mL of rIL-7 and 5 ng/mL rIL-15. All unique materials are available from the authors upon request.

The methodology to expand human NK cells has been described previously⁵⁵. Briefly, we co-cultured *CD56*⁺ PBMCs (enriched via positive magnetic column selection) with irradiated *K562-mb15-41BBL* at a 1:10 (NK cell:*K562*) in G-Rex cell culture devices (Wilson Wolf) in Stem Cell Growth Medium (CellGenix) supplemented with 500 IU/mL recombinant human interleukin-2 (NIH).

Co-culture experiments. *FfLuc*-expressing cancer cells were seeded in 48-well plates. We added either non-transduced T cells, *HER2.CARTs*, or NK cells 24 h later at the ratios described in Figure legends. We measured residual live cells (*ffLuc* activity) using a Luciferase Assay System (Promega) and measured by plate reader (BMG Labtech) at time points described in the Figure legends. We measured amounts of Granulysin using a granulysin ELISA kit (R&D).

Flow cytometry. We used the following fluorochrome-conjugated monoclonal antibodies: anti-human CD3, CD4, CD8, CD25, CD69, CD134, CD137, CCR7, CD45RO, PD-1, PD-L1, HER2, CD20, CD56, CD14, CD33, *NKG2C*, recombinant human HER2-Fc chimera, and anti-Fc (for detection of *HER2.CAR*) (BD Bioscience, Beckman Coulter, BioLegend, R&D systems). Cells were stained with these Abs or the appropriate isotype controls Abs for 30 min at 4 °C. We determined live/dead discrimination via exclusion of 7AAD positive cells (BD Pharmingen). Stained cells were analyzed using a Gallios flow cytometer (Beckman Coulter). We analyzed data with Kaluza software (BD Bioscience) according to the manufacturer's instructions.

Animal experiments. The Baylor College of Medicine Institutional Animal Care and Use Committee approved all animal experiments.

For the subcutaneous models, 2×10^6 CFPAC-1 cells or 5×10^6 CAPAN-1 cells were resuspended in a volume of 100 μL of PBS and injected into the right flank of 7–8 week-old NSG male or female mice. Fourteen days post transplantation, a total of 1×10^7 vp of *CAd* (*OAd:HDAd*=1:1) were injected in a volume of 20 μL into the tumor. The ratio of *OAd* to *HDAd* in the *CAd* system was optimized to effectively propagate transgene(s) encoded in the co-injected *HDAd* with lytic effects even with clinically relevant dosages. Three days post injection of *CAd*s, mice received 1×10^6 *HER2.CARTs* intravenously. *CARTs* expressing *ffLuc* were assessed using the *In Vivo Imaging System* (Xenogen)¹³. The endpoint was established at a tumor volume > 1500 mm^3 .

For the humanized mouse model, Newborn (1–2 day from birth) female and male *NSGSGM3* (*NSGTG*^{CMV-IL3,CSF2,KITLG Eav/ml0ySz; Jackson Laboratory) were sublethally irradiated (100 cGy) and intrahepatically injected with 5×10^4 human cord-blood unit (CBU)-derived *CD34*⁺ cells. CBUs were obtained from MD Anderson Stem Cell Center, and *CD34*⁺ cells were isolated using *CD34*⁺ cell isolation kit (Miltenyi Biotec Inc.). After confirming human *CD45*⁺ cells in PBMCs of mice 8–9 weeks post injection, 2×10^6 CFPAC-1 cells were resuspended in a volume of 100 μL of PBS and injected into the right flank of male and female humanized mice. Eighteen days post transplantation, a total of 1×10^7 vp of *CAd* (*OAd:HDAd*=1:1) were injected in a volume of 20 μL into the tumor. Three days post injection of *CAd*s, mice received 1×10^6 autologous *HER2.CARTs* (same CBU derived PBMCs) intravenously. *CARTs* expressing *ffLuc* were assessed using the *In*}

Vivo Imaging System (Xenogen)¹³. The endpoint was established at a tumor volume > 1500 mm³.

For humanized mice with two CFPAC-1 tumors per mouse, we injected 2 × 10⁶ CFPAC-1 cells into the right flank and 1 × 10⁶ CFPAC-1 cells into the left flank. Eighteen days post transplantation, we injected a total of 1 × 10⁷ vp of CAD (OAd: HDAd=1:1) into the right flank tumor. Three days post injection of CADs, mice received 1 × 10⁶ autologous HER2.CARTs intravenously. The endpoint was established at combined tumor volumes (right tumor volume plus left tumor volume) > 1500 mm³.

Isolation of tumor-infiltrating immune cells. After rinsing harvested tumors with PBS, tumors were minced and incubated in RPMI media containing human tumor dissociation reagents (Miltenyi Biotech Inc.) at 37 °C for 1 h. Cells were passed through a 70-µm cell strainer (BD Pharmingen), and murine stroma cells were removed using a Mouse Cell Depletion kit (Miltenyi Biotech Inc.). Human cells were stained with the antibodies described in Results.

RNA extraction and RT-PCR. CFPAC-1 tumors were harvested from non-humanized and humanized mice 3 days post injection of CAD_{Trio}, and RNA was extracted from whole tumors using RNeasy Plus Mini kit (Qiagen). RNA samples were converted to cDNA using Super Script III First-Strand Synthesis System (Thermo Fisher). The levels of human pro-inflammatory cytokine/chemokine described in Results were quantified using CFX96 Real-Time PCR Detection System (Bio-Rad) and normalized with human β-Actin. We obtained all primer sets from Bio-Rad.

Microarray analysis. We harvested CFPAC-1 tumors from humanized mice 31 days post injection of CAD_{Trio}. Total RNA was extracted from whole tumors using the RNeasy Plus Mini kit and quantified using the NanoDrop 2000 (Thermo Fisher Scientific Inc.). The Baylor Genomic & RNA Profiling Core performed RNA expression profiling with the nCounter Human Immunology V2 Panel (NanoString Technologies). Data quality control, normalization, and advanced analysis were performed using nSolver 4.0 analysis software following NanoString analysis guidelines. Supplementary gene expression tables show expression level >2 and *p* < 0.05.

Quantification of vector genome DNA in Ad infected tumors. We harvested PDAC tumors at time points described in the Figure legends. Total DNA was extracted from infected tumors, and vector copies were quantified with primer sets for OAd (5'- TCCGGTTTCTATGCCAACCT-3' and 5'- TCCTCCGGTGA-TAATGACAAGA-3') and HDAd (5'-TCTGAATAATTTGTGTTACTCA-TAGCGCG-3' and 5'-CCCATAAGCTCCTTTAACTTGTTAAAGTC-3') and normalized with murine genomic GAPDH (5'- TAGGCCAGGATGTAAGGT-CATTAAG-3' and 5'- CCAGAAAGTCCACACGGCTAAA-3')¹⁰.

Immunohistochemistry. The Human Tissue Acquisition and Pathology Core at Baylor College of Medicine stained CFPAC-1 tumors from xenograft and humanized mice with anti-human CD45 antibody.

Statistics and reproducibility. Results are represented as means of twice or more independent experiments (biological replication). Data with three or more groups were analyzed by ordinary one-way ANOVA analysis. Wilcoxon matched pairs test was used to compare two groups of paired data. Data were analyzed with GraphPad Prism 9.

Reporting summary. Further information on research design is available in the Nature Research Reporting Summary linked to this article.

Data availability

The Nanostring data are available on NCBI GEO (GEO accession number: GSE167113). Source data are available as Supplementary Data 4. All other data are available from the authors on reasonable request.

Received: 17 September 2020; Accepted: 23 February 2021;

Published online: 19 March 2021

References

1. Ferlay, J. et al. Cancer incidence and mortality patterns in Europe: estimates for 40 countries and 25 major cancers in 2018. *Eur. J. Cancer* **103**, 356–387 (2018).
2. Calabrese, C. et al. Genomic basis for RNA alterations in cancer. *Nature* **578**, 129–136 (2020).
3. Kabacaoglu, D., Ciecieski, K. J., Ruess, D. A. & Algul, H. Immune checkpoint inhibition for pancreatic ductal adenocarcinoma: current limitations and future options. *Front. Immunol.* **9**, 1878 (2018).
4. Harrington, K., Freeman, D. J., Kelly, B., Harper, J. & Soria, J. C. Optimizing oncolytic virotherapy in cancer treatment. *Nat. Rev. Drug Discov.* **18**, 689–706 (2019).
5. Harrington, K. J. et al. Clinical development of talimogene laherparepvec (T-VEC): a modified herpes simplex virus type-1-derived oncolytic immunotherapy. *Expert Rev. Anticancer Ther.* **15**, 1389–1403 (2015).
6. Noonan, A. M. et al. Randomized phase 2 Trial of the oncolytic virus pelareorep (reolysin) in upfront treatment of metastatic pancreatic adenocarcinoma. *Mol. Ther.* **24**, 1150–1158 (2016).
7. Haas, A. R. et al. Phase I study of lentiviral-transduced chimeric antigen receptor-modified T cells recognizing mesothelin in advanced solid cancers. *Mol. Ther.* **27**, 1919–1929 (2019).
8. Aumayr, K. et al. HER2 gene amplification and protein expression in pancreatic ductal adenocarcinomas. *Appl. Immunohistochem. Mol. Morphol.* **22**, 146–152 (2014).
9. Harder, J. et al. Multicentre phase II trial of trastuzumab and capecitabine in patients with HER2 overexpressing metastatic pancreatic cancer. *Br. J. Cancer* **106**, 1033–1038 (2012).
10. Farzad, L. et al. Combinatorial treatment with oncolytic adenovirus and helper-dependent adenovirus augments adenoviral cancer gene therapy. *Mol. Ther. Oncolytics* **1**, 14008 (2014).
11. Ahmed, N. et al. Human Epidermal Growth Factor Receptor 2 (HER2)-specific chimeric antigen receptor-modified T cells for the immunotherapy of HER2-positive sarcoma. *J. Clin. Oncol.* **33**, 1688–1696 (2015).
12. Ahmed, N., et al. HER2-specific chimeric antigen receptor-modified virus-specific T cells for progressive glioblastoma: a phase 1 dose-escalation trial. *JAMA Oncol.* **3**, 1094–1101 (2017).
13. Tanoue, K., et al. Armed oncolytic adenovirus expressing PD-L1 mini-body enhances anti-tumor effects of chimeric antigen receptor T-cells in solid tumors. *Cancer Res.* **77**, 2040–2051 (2017).
14. Roswell Shaw, A. et al. Adenovirotherapy delivering cytokine and checkpoint inhibitor augments CAR T cells against metastatic head and neck cancer. *Mol. Ther.* **25**, 2440–2451 (2017).
15. Porter, C. E. et al. Oncolytic adenovirus armed with BiTE, cytokine, and checkpoint inhibitor enables CAR T cells to control the growth of heterogeneous tumors. *Mol. Ther.* **28**, 1251–1262 (2020).
16. Conry, R. M., Westbrook, B., McKee, S. & Norwood, T. G. Talimogene laherparepvec: first in class oncolytic virotherapy. *Hum. Vaccines Immunother.* **14**, 839–846 (2018).
17. Mahalingam, D., et al. A phase II study of pelareorep (REOLYSIN((R))) in combination with gemcitabine for patients with advanced pancreatic adenocarcinoma. *Cancers* **10**, 160 (2018).
18. Salmon, H., Remark, R., Gnjatic, S. & Merad, M. Host tissue determinants of tumour immunity. *Nat. Rev. Cancer* **19**, 215–227 (2019).
19. Wang, H. et al. A new human DSG2-transgenic mouse model for studying the tropism and pathology of human adenoviruses. *J. Virol.* **86**, 6286–6302 (2012).
20. Jogler, C. et al. Replication properties of human adenovirus in vivo and in cultures of primary cells from different animal species. *J. Virol.* **80**, 3549–3558 (2006).
21. Ahmed, N. et al. Regression of experimental medulloblastoma following transfer of HER2-specific T cells. *Cancer Res.* **67**, 5957–5964 (2007).
22. Norelli, M. et al. Monocyte-derived IL-1 and IL-6 are differentially required for cytokine-release syndrome and neurotoxicity due to CAR T cells. *Nat. Med.* **24**, 739–748 (2018).
23. Hong, M. et al. Chemotherapy induces intratumoral expression of chemokines in cutaneous melanoma, favoring T-cell infiltration and tumor control. *Cancer Res.* **71**, 6997–7009 (2011).
24. Harlin, H. et al. Chemokine expression in melanoma metastases associated with CD8+ T-cell recruitment. *Cancer Res.* **69**, 3077–3085 (2009).
25. Shaw, A. R. & Suzuki, M. Immunology of adenoviral vectors in cancer therapy. *Mol. Ther. Methods Clin. Dev.* **15**, 418–429 (2019).
26. Roswell Shaw, A. & Suzuki, M. Oncolytic viruses partner with T-cell therapy for solid tumor treatment. *Front. Immunol.* **9**, 2103 (2018).
27. Li, A. et al. Activating cGAS-STING pathway for the optimal effect of cancer immunotherapy. *J. Hematol. Oncol.* **12**, 35 (2019).
28. Evgin, L. et al. Oncolytic virus-derived type I interferon restricts CAR T cell therapy. *Nat. Commun.* **11**, 3187 (2020).
29. Suzuki, M. et al. Differential type I interferon-dependent transgene silencing of helper-dependent adenoviral vs. adeno-associated viral vectors in vivo. *Mol. Ther.* **21**, 796–805 (2013).
30. Xu, N., et al. STING agonist promotes CAR T cell trafficking and persistence in breast cancer. *J. Exp. Med.* **218**, e20200844 (2021).
31. Suzuki, M. et al. MyD88-dependent silencing of transgene expression during the innate and adaptive immune response to helper-dependent adenovirus. *Hum. Gene Ther.* **21**, 325–336 (2010).

32. Spranger, S., Dai, D., Horton, B. & Gajewski, T. F. Tumor-residing Batf3 dendritic cells are required for effector T cell trafficking and adoptive T cell therapy. *Cancer Cell* **31**, 711–723 e714 (2017).
33. Siegel, R. L., Miller, K. D. & Jemal, A. Cancer statistics, 2016. *CA* **66**, 7–30 (2016).
34. Ma, M. et al. NKG2C(+)NKG2A(-) natural killer cells are associated with a lower viral set point and may predict disease progression in individuals with primary HIV infection. *Front. Immunol.* **8**, 1176 (2017).
35. Guma, M. et al. The CD94/NKG2C killer lectin-like receptor constitutes an alternative activation pathway for a subset of CD8+ T cells. *Eur. J. Immunol.* **35**, 2071–2080 (2005).
36. Muller, L., Aigner, P., Stoiber, D. & Type, I. Interferons and natural killer cell regulation in cancer. *Front. Immunol.* **8**, 304 (2017).
37. Teng, M. W. et al. IL-12 and IL-23 cytokines: from discovery to targeted therapies for immune-mediated inflammatory diseases. *Nat. Med.* **21**, 719–729 (2015).
38. Pesce, S. et al. PD-1/PD-Ls checkpoint: insight on the potential role of NK cells. *Front. Immunol.* **10**, 1242 (2019).
39. Weber, E. W., Maus, M. V. & Mackall, C. L. The emerging landscape of immune cell therapies. *Cell* **181**, 46–62 (2020).
40. Raj, D. et al. Switchable CAR-T cells mediate remission in metastatic pancreatic ductal adenocarcinoma. *Gut* **68**, 1052–1064 (2019).
41. Watanabe, N. et al. Fine-tuning the CAR spacer improves T-cell potency. *Oncoimmunology* **5**, e1253656 (2016).
42. Kershaw, M. H. et al. A phase I study on adoptive immunotherapy using gene-modified T cells for ovarian cancer. *Clin. Cancer Res.* **12**, 6106–6115 (2006).
43. Metzger, P. et al. Immunostimulatory RNA leads to functional reprogramming of myeloid-derived suppressor cells in pancreatic cancer. *J. Immunother. Cancer* **7**, 288 (2019).
44. Kuryk, L., Moller, A. W. & Jaderberg, M. Abscopal effect when combining oncolytic adenovirus and checkpoint inhibitor in a humanized NOG mouse model of melanoma. *J. Med. Virol.* **91**, 1702–1706 (2019).
45. Chon, H. J. et al. Tumor microenvironment remodeling by intratumoral oncolytic vaccinia virus enhances the efficacy of immune-checkpoint blockade. *Clin. Cancer Res.* **25**, 1612–1623 (2019).
46. Leoni, V. et al. A fully-irulent retargeted oncolytic HSV armed with IL-12 elicits local immunity and vaccine therapy towards distant tumors. *PLoS Pathog.* **14**, e1007209 (2018).
47. Andtbacka, R. H. et al. Talimogene laherparepvec improves durable response rate in patients with advanced melanoma. *J. Clin. Oncol.* **33**, 2780–2788 (2015).
48. Cerwenka, A. & Lanier, L. L. Natural killer cell memory in infection, inflammation and cancer. *Nat. Rev. Immunol.* **16**, 112–123 (2016).
49. Lim, S. A. et al. Defective localization with impaired tumor cytotoxicity contributes to the immune escape of NK cells in pancreatic cancer patients. *Front. Immunol.* **10**, 496 (2019).
50. Tang, Y. P. et al. Prognostic value of peripheral blood natural killer cells in colorectal cancer. *BMC Gastroenterol.* **20**, 31 (2020).
51. Muthalagu, N. et al. Repression of the type I interferon pathway underlies MYC- and KRAS-dependent evasion of NK and B cells in pancreatic ductal adenocarcinoma. *Cancer Discov.* **10**, 872–887 (2020).
52. Skelton, J. K., Ortega-Prieto, A. M. & Dorner, M. A Hitchhiker's guide to humanized mice: new pathways to studying viral infections. *Immunology* **154**, 50–61 (2018).
53. Suzuki, M. et al. Large-scale production of high-quality helper-dependent adenoviral vectors using adherent cells in cell factories. *Hum. Gene Ther.* **21**, 120–126 (2010).

54. Guse, K. et al. Capsid-modified adenoviral vectors for improved muscle-directed gene therapy. *Hum. Gene Ther.* **23**, 1065–1070 (2012).
55. Parihar, R. et al. NK cells expressing a chimeric activating receptor eliminate MDSCs and rescue impaired CAR-T cell activity against solid tumors. *Cancer Immunol. Res.* **7**, 363–375 (2019).

Acknowledgements

The authors would like to thank Catherine Gillespie in the Center for Cell and Gene Therapy at Baylor College of Medicine for her editing of the paper. This work was supported by Tessa Therapeutics Pte. This work was also supported by NIH P01 CA094237 to M.K. Brenner, NIH P30-CA125123 to Human Tissue Acquisition and Pathology Core, NIH 5T32HL092332-17 to Dr. Helen Heslop and HHSH75R60219C00004 to MD Anderson Cord Blood Bank. Dysthe was supported by NIH 5T32GM088129-10. The content is solely the responsibility of the authors and does not necessarily represent the official views of the NIH.

Author contributions

Conceptualization, M.S.; methodology, A.R., C.E.P., T.Y., W.-C.M., M.K.M., Y.J., and M. D.; investigation, A.R., C.E.P., T.Y., W.-C.M., M.K.M., Y.J., M.D., R.P., and M.S.; writing—original draft, A.R. and M.S.; writing—review & editing, M.S. and M.K.B.; supervision, M.S.; funding acquisition, M.K.B. and M.S.

Competing interests

M.S. is a scientific consultant, and C.E.P. is a consultant for Tessa Therapeutic Ltd. The other authors declare no competing interest.

Additional information

Supplementary information The online version contains supplementary material available at <https://doi.org/10.1038/s42003-021-01914-8>.

Correspondence and requests for materials should be addressed to M.S.

Reprints and permission information is available at <http://www.nature.com/reprints>

Publisher's note Springer Nature remains neutral with regard to jurisdictional claims in published maps and institutional affiliations.



Open Access This article is licensed under a Creative Commons Attribution 4.0 International License, which permits use, sharing, adaptation, distribution and reproduction in any medium or format, as long as you give appropriate credit to the original author(s) and the source, provide a link to the Creative Commons license, and indicate if changes were made. The images or other third party material in this article are included in the article's Creative Commons license, unless indicated otherwise in a credit line to the material. If material is not included in the article's Creative Commons license and your intended use is not permitted by statutory regulation or exceeds the permitted use, you will need to obtain permission directly from the copyright holder. To view a copy of this license, visit <http://creativecommons.org/licenses/by/4.0/>.

© The Author(s) 2021